Correlating Molecular Structure to Field-Effect Mobility: The Investigation of Side-Chain Functionality in Phenylene−Thiophene Oligomers and Their Application in Field Effect Transistors

Andrew Sung,[†] Mang Mang Ling,[†] Ming Lee Tang,[†] Zhenan Bao,*[,†] and Jason Locklin*[,‡]

Department of Chemical Engineering, Stanford University, 381 North South Mall, Stanford, California 94305, and Department of Chemistry and Faculty of Engineering, University of Georgia, Athens, Georgia 30602

Received January 12, 2007. Revised Manuscript Received February 22, 2007

Short conjugated phenylene (P)−thiophene (T) oligomers with varying α and ω alkyl and alkoxy substitutions were synthesized using Stille and Suzuki coupling reactions to investigate the correlation between end-group structure and electronic properties on P2TP and P3TP conjugated cores. Several soluble oligomers were synthesized with 5,5′-bis(4-*n*-octylphenyl)-2,2′-bithiophene (do-PTTP) showing the highest mobility ($\mu = 0.18$ cm^2 V^{-1} s^{-1}) and on/off ratio of 10^7 at a substrate temperature of 50 °C. Thin film morphologies analyzed using atomic force microscopy revealed higher nucleation densities for branched alkoxy side-chain molecules compared to those of their straight alkyl side-chain counterparts. Field-effect mobility showed an inverse correlation to side-group bulkiness, indicating a strong morphological component to charge transport in the P2TP and P3TP series.

Introduction

There is a tremendous interest in using organic semiconductors for electronic devices, some of which include sensors, smart tags, and displays that are low cost and large area.[1−3] Several different oligomeric and polymeric semiconductor backbones have been synthesized for use in organic field-effect transistors (OFETs), with field-effect mobility values comparable to that of amorphous silicon.[4−11] The relationship between solid-state crystallinity and electronic performance is well established, but there are many critical factors that are not understood in terms of molecular design, where subtle changes in intermolecular interactions can lead to dramatic changes in thin film morphology and crystallinity, which in turn alter the electronic properties. A large amount of work, in terms of synthetic design, has gone into "tuning" the organic semiconductor core, both to optimize charge transport and maintain environmental stability.[5,6,12,13] One example where crystal structure variation has been studied intensely is the family of linear acenes, which is the subject of a recent review.[14] Most of the time, alkyl substituents are added to the semiconductor backbone in order to impart solubility and influence the thin film microstructure at the semiconductor/insulator interface.

The side chains present on a molecule play an important role in determining the thin film microstructure at the semiconductor−dielectric interface in an organic thin film transistor. The first studies on molecular substitution were performed on oligothiophenes by Garnier et al.[15] Hexyl side chains were substituted at the α- and ω-positions of the sexithiophene ring system. It was observed that the field-effect mobility in the thin film transistor geometry increased by a factor of 25 over the unsubstituted sexithiophene, and this was attributed to enhanced self-assembly properties of the alkyl chains. Since then, others have introduced alkyl side chains onto other semiconductor backbones, where similar improvements in device performance have been observed.[6,16,17] The ability to solution cast semiconductor

* Corresponding authors. E-mail: zbao@stanford.edu (Z.B.); jlocklin@chem.uga.edu (J.L.).
[†] Stanford University.
[‡] University of Georgia.

(1) Subramanian, V.; Chang, P. C.; Lee, J. B.; Molesa, S. E.; Volkman, S. K. *IIEEE Trans. Compon. Packag. Technol.* **2005**, *28*, 742−747.
(2) Byungwook, Y.; Taeho, J.; Debarshi, B.; Ananth, D.; Brooks, A. J.; Antonio, F.; Michael, R. W.; Tobin, J. M. *Appl. Phys. Lett.* **2006**, *88*, 082104.
(3) Drury, C. J.; Mutsaers, C. M. J.; Hart, C. M.; Matters, M.; de Leeuw, D. M. *Appl. Phys. Lett.* **1998**, *73*, 108−110.
(4) Mcculloch, I.; Heeney, M.; Bailey, C.; Genevicius, K.; Macdonald, I.; Shkunov, M.; Sparrowe, D.; Tierney, S.; Wagner, R.; Zhang, W. M.; Chabinyc, M. L.; Kline, R. J.; Mcgehee, M. D.; Toney, M. F. *Nat. Mater.* **2006**, *5*, 328−333.
(5) Locklin, J.; Ling, M. M.; Sung, A.; Roberts, M. E.; Bao, Z. N. *Adv. Mater.* **2006**, *18*, 2989.
(6) Meng, H.; Bao, Z. N.; Lovinger, A. J.; Wang, B. C.; Mujsce, A. M. *J. Am. Chem. Soc.* **2001**, *123*, 9214−9215.
(7) Meng, H.; Sun, F. P.; Goldfinger, M. B.; Gao, F.; Londono, D. J.; Marshal, W. J.; Blackman, G. S.; Dobbs, K. D.; Keys, D. E. *J. Am. Chem. Soc.* **2006**, *128*, 9304−9305.
(8) Meng, H.; Sun, F. P.; Goldfinger, M. B.; Jaycox, G. D.; Li, Z. G.; Marshall, W. J.; Blackman, G. S. *J. Am. Chem. Soc.* **2005**, *127*, 2406−2407.
(9) Payne, M. M.; Parkin, S. R.; Anthony, J. E.; Kuo, C. C.; Jackson, T. N. *J. Am. Chem. Soc.* **2005**, *127*, 4986−4987.
(10) Letizia, J. A.; Facchetti, A.; Stern, C. L.; Ratner, M. A.; Marks, T. J. *J. Am. Chem. Soc.* **2005**, *127*, 13476−13477.
(11) Yoon, M. H.; DiBenedetto, S. A.; Facchetti, A.; Marks, T. J. *J. Am. Chem. Soc.* **2005**, *127*, 1348−1349.
(12) Anthony, J. E.; Brooks, J. S.; Eaton, D. L.; Parkin, S. R. *J. Am. Chem. Soc.* **2001**, *123*, 9482−9483.
(13) Heeney, M.; Bailey, C.; Genevicius, K.; Shkunov, M.; Sparrowe, D.; Tierney, S.; McCulloch, I. *J. Am. Chem. Soc.* **2005**, *127*, 1078−1079.
(14) Anthony, J. E. *Chem. Rev.* **2006**, *106*, 5028−5048.
(15) Garnier, F.; Yassar, A.; Hajlaoui, R.; Horowitz, G.; Deloffre, F.; Servet, B.; Ries, S.; Alnot, P. *J. Am. Chem. Soc.* **1993**, *115*, 8716−8721.
(16) Katz, H. E.; Lovinger, A. J.; Laquindanum, J. G. *Chem. Mater.* **1998**, *10*, 457−459.

10.1021/cm070117n CCC: $37.00
Published on Web 04/05/2007

films introduces the possibility of high-throughput processing, such as ink-jet printing, and has largely been the driving force behind developing soluble organic semiconductors. Bulky side chains have been introduced to oligothiophene systems in order to improve solubility, but this causes a drastic decrease in device performance.[18] The same intermolecular forces that provide desirable electronic properties are also the ones that inhibit solubility (and solution processability) in organic solvents. Recently, we have investigated the substitution of cyclohexyl side chains on several different organic semiconductors, which improve solubility while maintaining excellent device performance.[19] This naturally leads to the question of just how bulky the substituent can be for a given semiconductor core. Where is the cutoff between improvements in solubility and the influence on device performance? In this paper, we have systematically investigated the effect of different end substitutions on a series of organic semiconductors based on a simple phenylene−thiophene core.

The Katz group has previously reported unsubstituted and alkyl-substituted phenylene−thiophene oligomers with field-effect mobilities as high as $\sim$0.1 $cm^2\ V^{-1}\ s^{-1}$, both from vacuum deposition and short-channel solution-processed devices.[20−22] This class of materials can also be transformed into n-channel or ambipolar transistors by modification with the appropriate end substitutions.[23] Because of these promising electronic properties and the ease of synthesis, we chose to use this semiconductor core to systematically study the effect of side-chain functionality using alkyl and alkoxy substituents. More than 20 molecules were synthesized with a variety of alkyl and alkoxy substituents in order to investigate the degree of substituent bulkiness and the effect of different side chains on thin film microstructure and device performance. With the use of the results, several general conclusions can be drawn that will prove useful in designing organic semiconductor molecules in the future.

Experimental Section

Chemicals and Methods. All chemical were purchased from Aldrich Chemical Co. unless otherwise stated. Boronic acid compounds were purchased from Combi-Blocks, Inc. 4-Bromo-1-alkylbenzene and 4-bromo-1-alkoxybenzene compounds were purchased from TCI Inc. Solvents were purchased from Fisher.

Vacuum Sublimation. Final purification of most oligomers was completed by vacuum sublimation under reduced pressure. A 1 in. diameter quartz crystal tube with 2 in. long quartz insert sleeves was placed into a Lindberg/Blue oven regulated by a Lindberg/Blue three-zone temperature controller. An attached Varian Turbo-V 250 turbo pump achieved vacuum pressures of $\sim 10^{-6}$ torr.

Table 1. X-ray Diffraction Obtained *d*-Spacing and Calculated Molecular Length

molecule	*d*-spacing (Å)	MM2-minimized length (Å)
dip-P2TP	21.8	25
dmo-P2TP	10.4	21
dtbo-P2TP	20.3	23
dtb-P2TP	15.8	21
dho-P2TP	32.2	32
dpo-P3TP	29.2	30
dho-P3TP	36.4	36
doo-P3TP	40.7	40

Instrumentation. ^{1}H nuclear magnetic resonance (NMR) spectra were obtained on Varian Gemini 200, Varian 400, and Inova 500 spectrometers at 200, 400, and 500 MHz, respectively. Chemical shifts (δ) are presented in parts per million using residual solvent as an internal standard ($CHCl_3$, $\delta = 7.26$).

Atomic Force Microscopy. A Digital Instruments MMAFM-2 scanning probe microscope was used to perform tapping mode atomic force microscopy (AFM) on the samples with a silicon tip of 300 kHz frequency. The 5 μm × 5 μm and 20 μm × 20 μm scans were completed on 2 nm films deposited on both bare SiO_2 and octadecyltrimethoxysilane (OTS)-treated SiO_2.

X-ray Diffraction. A Philips PANalytical X'Pert diffractometer with a PreFIX X-ray mirror at the incident beam and a parallel plate collimator at the diffracted beam was used on the thin films of the evaporated molecules. The $\omega/2\theta$ scans were performed with Cu Kα radiation at a power of 45 mV and 40 mA, with a step size of 0.02° and a step time of 10 s.

Cyclic Voltammetry. Highest occupied molecular orbital (HOMO) levels were measured using cyclic voltammetry on a CHI411 CH Instruments analyzer. Cyclic voltammetry was performed on a solution saturated with the corresponding oligomer (0.1 M tetrabutylammonium hexafluorophosphate (Bu_4NPF_6) in anhydrous methylene chloride (CH_2Cl_2) solution), sweeping from −0.2 to 1.5 V at a differential scan rate of 50 mV/s. A Ag quasi-reference electrode and Pt working/counter electrode were used. The ferrocene/ferrocenium redox couple was used as an internal standard in each case.

Deposition/Device Fabrication. Top contact devices were made according to a literature procedure.[5] The n-doped silicon substrate functions as the gate electrode, while a thermally grown 300 nm silicon dioxide layer with a capacitance per unit area of 1.0×10^{-8} F/cm^2 functions as the dielectric. Shadow masks with W/L of 20 ($W = 4000$ μm, $L = 200$ μm) were used after the evaporation of the organic semiconductor to deposit the gold electrodes. The organic semiconductors were deposited at a rate of 1 Å/s under a pressure of 6×10^{-6} mm of Hg to a final thickness of 45−50 nm as determined by a quartz crystal monitor. Transistor measurements were performed in air using a Keithley 2400 semiconductor parameter analyzer. I_{DS} was measured as V_G was swept from +20 to −100 V at a constant V_{DS} of −100 V. Mobility values reported were calculated from the saturation regime.[24,25] At least six top contact transistor devices from the same substrate were tested for each molecule, and the average value and standard deviation of each parameter are reported below. Devices were fabricated at different substrate temperatures, and the best mobility values for each oligomer are shown in Tables 2 and 3. Each batch contained

(17) Malenfant, P. R. L.; Dimitrakopoulos, C. D.; Gelorme, J. D.; Kosbar, L. L.; Graham, T. O.; Curioni, A.; Andreoni, W. *Appl. Phys. Lett.* **2002**, *80*, 2517−2519.
(18) Barbarella, G.; Ostoja, P.; Maccagnani, P.; Pudova, O.; Antolini, L.; Casarini, D.; Bongini, A. *Chem. Mater.* **1998**, *10*, 3683−3689.
(19) Locklin, J.; Li, D. W.; Mannsfeld, S. C. B.; Borkent, E. J.; Meng, H.; Advincula, R.; Bao, Z. *Chem. Mater.* **2005**, *17*, 3366−3374.
(20) Hong, X. M.; Katz, H. E.; Lovinger, A. J.; Wang, B. C.; Raghavachari, K. *Chem. Mater.* **2001**, *13*, 4686−4691.
(21) Mushrush, M.; Facchetti, A.; Lefenfeld, M.; Katz, H. E.; Marks, T. J. *J. Am. Chem. Soc.* **2003**, *125*, 9414−9423.
(22) Katz, H. E.; Siegrist, T.; Lefenfeld, M.; Gopalan, P.; Mushrush, M.; Ocko, B.; Gang, O.; Jisrawl, N. *J. Phys. Chem. B* **2004**, *108*, 8567−8571.
(23) Facchetti, A.; Letizia, J.; Yoon, M. H.; Mushrush, M.; Katz, H. E.; Marks, T. J. *Chem. Mater.* **2004**, *16*, 4715−4727.
(24) Newman, C. R.; Frisbie, C. D.; daSilvaFilho, D. A.; Bredas, J. L.; Ewbank, P. C.; Mann, K. R. *Chem. Mater.* **2004**, *16*, 4436−4451.
(25) Dimitrakopoulos, C. D.; Brown, A. R.; Pomp, A. *J. Appl. Phys.* **1996**, *80*, 2501−2508.

Table 2. Mobility, On/Off, and Threshold Voltage Data for P2TP Molecules

molecule	mobility ($cm^2\ V^{-1}\ s^{-1}$)	on/off	V_T (V)	substrate temp (°C)
dip-P2TP	0.026 ± 0.0006	4×10^6	-14.1 ± 1.1	40
dtb-P2TP	0.007 ± 0.0004	4×10^5	-16.3 ± 2.6	50
db-P2TP	0.14 ± 0.05	9×10^4	-5.8 ± 2.1	40
do-P2TP	0.18 ± 0.005	9×10^6	-17.3 ± 1.4	50
dmo-P2TP	no observed mobility			40
dipo-P2TP	0.046 ± 0.0004	3×10^3	-0.6 ± 1.1	40
dpo-P2TP	0.059 ± 0.0006	3×10^5	-8.2 ± 0.4	50
dbo-P2TP	0.07 ± 0.002	2×10^5	-3.3 ± 1.3	50
dtbo-P2TP	0.003 ± 0.0002	2×10^4	-3.9 ± 3.4	40
dho-P2TP	0.065 ± 0.001	6×10^5	-16.3 ± 0.8	50
doo-P2TP	0.18 ± 0.008	5×10^7	-5.4 ± 0.4	50

both plain and OTS-treated SiO_2 substrates, which were grown from OTS vapor at a reduced pressure in a closed container.

Oligomer Synthesis. The synthetic protocol for the oligomers used in this work is outlined in Schemes 1 and 2.

Synthesis of 5,5′-Bis(4-isopropylphenyl)-2,2′-bithiophene (dip-P2TP). To a solution of 4-isopropylphenylboronic acid (1.12 g, 6.82 mmol) and 2,2′-dibromobithiophene (1.15 g, 3.54 mmol) dissolved in toluene (15 mL) was added potassium carbonate (4.72 g, 34.2 mmol) dissolved in water (50 mL) followed by the addition of phase-transfer agent Aliquot 336 (1.3 g, 3.22 mmol). The mixture was bubbled with nitrogen for 15 min. Then, tetrakis(triphenylphosphine)palladium(0) (85 mg, 0.074 mmol) was added, and the mixture was bubbled with N_2 for an additional 10 min. The mixture was heated to 85 °C for 20 h under nitrogen. The precipitate was filtered and washed with methanol and further purified by flashing through a silica column with chloroform as eluent to give an orange solid (yield = 57.2%). ^{1}H NMR (500 MHz, $CDCl_3$): δ_H 7.54 (d, 4H, J = 8.0 Hz), 7.25 (d, 2H, J = 8.0 Hz), 7.19 (d, 2H, J = 3.8 Hz), 7.15 (d, 2H, 3.8 J = Hz), 2.93 (m, 2H), 1.28 (d, 2H, J = 7.1 Hz). ^{13}C NMR (500 MHz, $CDCl_3$, δ): 24.18, 31.12, 34.06, 123.56, 124.55, 125.86, 127.26, 131.91, 136.55, 143.45, 148.77. Anal. Calcd for $C_{26}H_{26}S_2$: C, 77.56; H, 6.51; S, 15.93. Found: C, 77.72; H, 6.48; S, 15.77.

5,5′-Bis(4-*tert*-butylphenyl)-2,2′-bithiophene (dtb-P2TP). The same procedure as above was used to give a yellow solid (yield = 82%). ^{1}H NMR (500 MHz, $CDCl_3$): δ_H 7.54 (d, 4H, J = 8.7 Hz), 7.41 (d, 4H, J = 8.7 Hz), 7.20 (d, 2H, J = 4.1 Hz), 7.15 (d, 2H, J = 4.1 Hz). ^{13}C NMR (400 MHz, $CDCl_3$, δ): 31.49, 34.87, 123.58, 124.52, 125.57, 126.10, 131.46, 136.66, 143.31, 150.97. Anal. Calcd for $C_{28}H_{30}S_2$: C, 78.09; H, 7.02; S, 14.89. Found: C, 78.10; H, 7.23; S, 14.77.

5,5′-Bis(4-methoxyphenyl)-2,2′-bithiophene (dmo-P2TP). The same procedure as above was used to give a yellow solid (yield = 81%). Anal. Calcd for $C_{22}H_{18}O_2S_2$: C, 69.81; H, 4.79; S, 16.94. Found: C, 69.79; H, 4.79; S, 16.56.

5,5′-Bis(4-isopropoxyphenyl)-2,2′-bithiophene (dipo-P2TP). The same procedure as above was used to give an orange solid (yield = 83%). Anal. Calcd for $C_{26}H_{26}O_2S_2$: C, 71.85; H, 6.29; S, 18.76. Found: C, 71.93; H, 5.79; S, 14.54.

5,5′-Bis(4-propoxyphenyl)-2,2′-bithiophene (dpo-P2TP). The same procedure as that for dip-P2TP was used. Instead of purification by column chromatography, the compound was purified using vacuum sublimation to give a yellow solid (yield = 80%). ^{1}H NMR (500 MHz, $CDCl_3$): δ_H 7.52 (d, 4H, J = 8.7 Hz), 7.11 (s, 4H), 6.91 (d, 4H, J = 8.7 Hz), 3.95 (t, 4H, J = 6.6 Hz), 1.83 (h, 4H, J = 6.1 Hz), 1.05 (t, 6H, J = 7.4 Hz). Anal. Calcd for $C_{26}H_{26}O_2S_2$: C, 71.85; H, 6.03; S, 14.76; O, 7.36. Found: C, 72.01; H, 6.22; S, 14.71.

5,5′-Bis(4-butoxyphenyl)-2,2′-bithiophene (dbo-P2TP). The same procedure as that for dip-P2TP was used. The bright yellow precipitate was filtered off, washed with methanol and chloroform (1.19 g, yield, 82%). ^{1}H NMR (500 MHz, $CDCl_3$): δ_H 7.51 (d, 4H, J = 8.7 Hz), 7.11 (m, 4H), 6.91 (d, 4H, J = 8.7 Hz), 4.00 (t, 4H, J = 6.5 Hz), 1.78 (p, 4H, J = 8 Hz), 1.50 (m, 4H), 0.99 (t, 6H, J = 7 Hz). Anal. Calcd for $C_{28}H_{30}O_2S_2$: C, 72.69; H, 6.54; S, 13.86; O, 6.92. Found: C, 72.47; H, 6.28; S, 13.86.

5,5′-Bis(4-hexyloxyphenyl)-2,2′-bithiophene (dho-P2TP). The same procedure as that for dip-P2TP was used. The filtered product was further purified by vacuum sublimation to yield a yellow solid (yield = 78%). Anal. Calcd for $C_{32}H_{38}O_2S_2$: C, 74.09; H, 7.38; S, 12.36. Found: C, 74.21; H, 7.31; S, 12.35.

5,5′-Bis(4-octyloxyphenyl)-2,2′-bithiophene (doo-P2TP). The same procedure as that for dip-P2TP was used. The filtered product was further purified by vacuum sublimation to yield a yellow solid (yield = 70%). ^{1}H NMR (500 MHz, $CDCl_3$): δ_H 7.52 (d, 4H, J = 8.0 Hz), 7.11 (s, 4H), 6.91 (d, 4H, J = 8.0 Hz), 3.98 (t, 4H, J = 6.5 Hz), 1.80 (m, 6H), 1.47 (m, 6H), 1.31 (m, 12H), 0.89 (t, 6H, J = 6.9 Hz). Anal. Calcd for $C_{36}H_{46}O_2S_2$: C, 75.21; H, 8.07; S, 11.16. Found: C, 74.92; H, 7.81; S, 11.37.

5,5′-Bis(4-*tert*-butoxyphenyl)-2,2′-bithiophene (dtbo-P2TP). To a nitrogen-evacuated flask was added 4-*tert*-butoxy-bromobenzene (0.83 g, 1.69 mmol) and 5,5′-bis-trimethylstannanyl-[2,2′]-bithiophene (0.77 g, 3.37 mmol). Anhydrous DMF (30 mL) was added via syringe, and the solution was bubbled with N_2 for 20 min. Then tetrakis(triphenylphosphine)palladium(0) (58 mg, 0.050 mmol) was added, and the solution was heated to 85 °C for 24 h. The solution was filtered, and the precipitate was washed with acetone to yield a yellow solid (0.58 g, yield = 75%). ^{1}H NMR (500 MHz, $CDCl_3$): δ_H 7.50 (d, 4H, J = 8.5 Hz), 7.15 (d, 2H, J = 3.5 Hz), 7.13 (d, 2H, J = 3.5 Hz), 7.01 (d, 4H, J = 8.5 Hz), 1.38 (s, 18H). ^{13}C NMR (500 MHz, $CDCl_3$, δ): 29.12, 79.22, 123.43, 124.568, 124.78, 126.43, 129.55, 136.48, 143.07, 155.40. Anal. Calcd for $C_{28}H_{30}O_2S_2$: C, 72.69; H, 6.54; S, 13.86. Found: C, 72.49; H, 6.28; S, 13.59.

5,5′-Bis(4-*n*-butylphenyl)-2,2′-bithiophene (db-P2TP). The same procedure as that for dtbo-P2TP was used. The compound was further purified by vacuum sublimation to yield a yellow solid (yield = 64%). ^{1}H NMR (500 MHz, $CDCl_3$): δ_H 7.52 (dd, 4H, ^3J = 6.5 Hz, ^4J = 2 Hz), 7.20 (m, 6H), 7.14 (d, 2H, J = 4 Hz), 2.63 (t, 4H, J = 7.7 Hz), 1.60 (m, 4H), 1.38 (h, 4H, J = 7.5 Hz), 0.94 (t, 6H, J = 7.2 Hz). ^{13}C NMR (500 MHz, $CDCl_3$, δ): 14.25, 22.62, 33.82, 35.62, 123.52, 124.54, 125.75, 129.24, 131.73, 136.52, 142.84, 143.45. Anal. Calcd for $C_{28}H_{30}S_2$: C, 78.09; H, 7.02; S, 14.89. Found: C, 78.12; H, 6.98; S, 14.67.

5,5′-Bis(4-*n*-octylphenyl)-2,2′-bithiophene (do-P2TP). The same procedure as that for db-P2TP was used to yield a yellow solid (yield = 77%). ^{1}H NMR (500 MHz, $CDCl_3$): δ_H 7.52 (d, 4H, J = 8.1 Hz), 7.29 (m, 6H), 7.14 (d, 2H, J = 3.6 Hz), 2.61 (t, 4H, J = 7.7 Hz), 1.60 (m, 4H), 1.30 (m, 20H), 0.88 (t, 6H, J = 6.8 Hz). ^{13}C NMR (500 MHz, $CDCl_3$, δ): 14.38, 22.94, 29.56, 29.74, 31.23, 31.70, 32.14, 35.94, 123.49, 124.52, 125.75, 129.20, 131.70, 136.53, 142.87, 143.45. Anal. Calcd for $C_{36}H_{46}S_2$: C, 79.65; H, 8.54; S, 11.81. Found: C, 79.44; H, 8.48; S, 11.63.

Preparation of 2,5″-Bis(4-isopropylphenyl)-2,2′:5′,2″-terthiophene (dip-P3TP). To a solution of 4-isopropylphenylboronic acid (0.266 g, 1.62 mmol) and 2,5″-dibromo-2,2′:5′,2″-terthiophene (0.33 g, 0.81 mmol) dissolved in toluene (15 mL) was added potassium carbonate (1.12 g, 8.1 mmol) dissolved in water (50 mL) followed by the addition of phase-transfer agent Aliquot 336 (0.33 g, 0.81 mmol). The mixture was bubbled with nitrogen for 15 min. Then, tetrakis(triphenylphosphine)palladium(0) (18.7 mg, 0.016 mmol) was added, and the mixture was bubbled with N_2 for an additional 10 min. The mixture was heated to 85 °C for 20 h under nitrogen. The bright yellow precipitate (yield = 81.5%) was filtered off, washed with methanol, and flashed through a silica column

Scheme 1. Synthesis of P2TP Derivatives with Various Side-Chain Functionalities

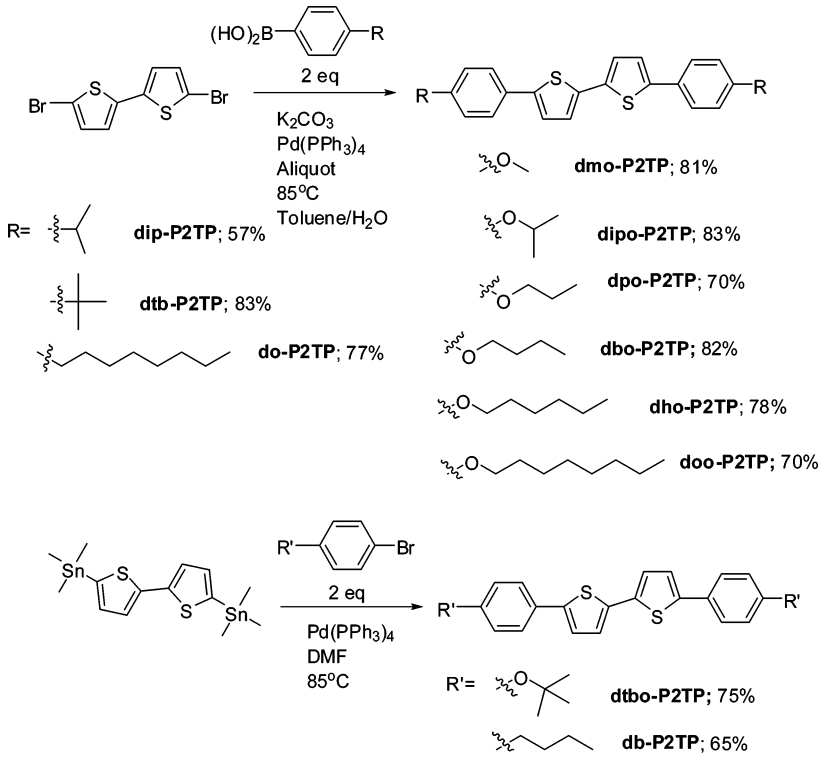

Scheme 2. Synthesis of P3TP Derivatives with Different Side-Chain Functionalities

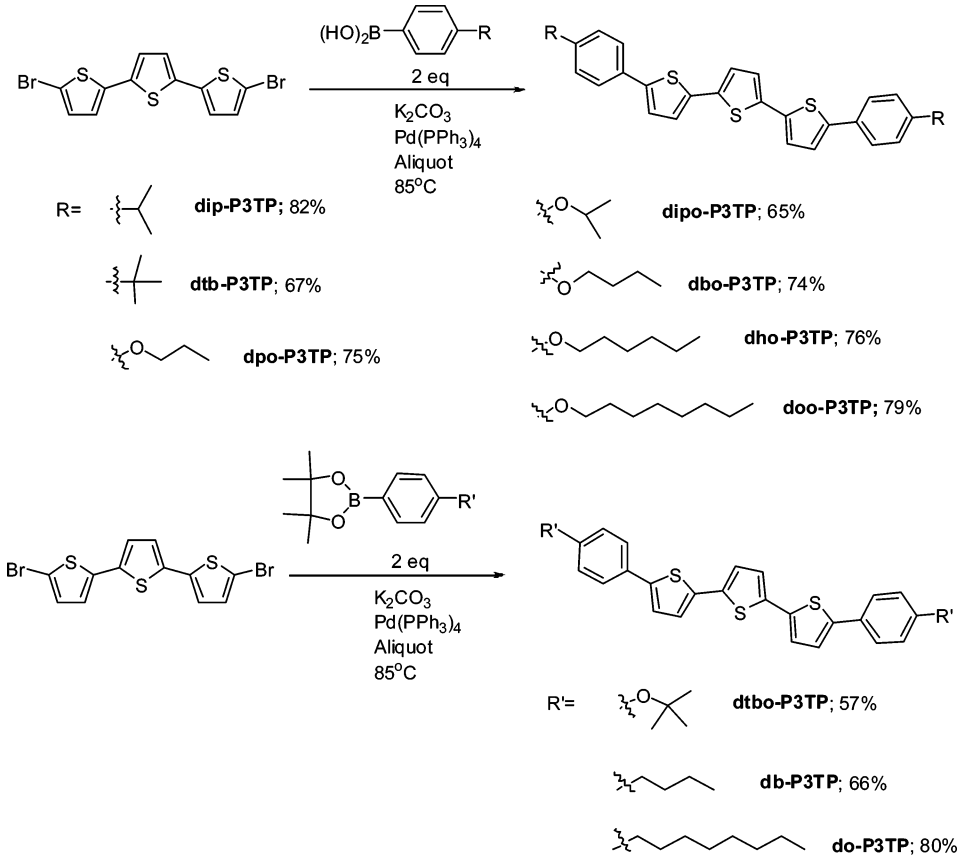

with chloroform as eluent. Anal. Calcd for $C_{30}H_{28}S_3$: C, 74.33; H, 5.82; S, 19.84. Found: C, 74.22; H, 5.80; S, 19.83.

2,5″-Bis(4-*tert*-butylphenyl)-2,2′:5′,2″-terthiophene (dtbu-P3TP). The same procedure as that for dip-P3TP was used to yield a flakey orange solid (yield = 63%). ^{1}H NMR (400 MHz, $CDCl_3$): δ_H 7.54 (d, 4H, J = 8.4 Hz), 7.41 (d, 4H, J = 8.4 Hz), 7.2 (d, 2H, J = 4.8 Hz), 7.14 (d, 2H, J = 4.8 Hz), 7.10 (s, 2H), 1.35 (s, 18H). Anal. Calcd for $C_{32}H_{32}S_3$: C, 74.95; H, 6.29; S, 18.76. Found: C, 74.95; H, 6.17; S, 18.70.

2,5″-Bis(4-propoxyphenyl)-2,2′:5′,2″-terthiophene (dpo-P3TP). The same procedure as that for dip-P3TP was used. The compound was flashed through a silica column to yield a waxy orange solid

(yield = 75%). Anal. Calcd for $C_{30}H_{28}O_2S_3$: C, 69.73; H, 5.46; O, 6.19; S, 18.62. Found: C, 69.79; H, 5.56; S, 18.61.

2,5″-Bis(4-isopropoxyphenyl)-2,2′:5′,2″-terthiophene (dipo-P3TP). The same procedure as that for dip-P3TP was used to yield an orange solid (yield = 65%). Anal. Calcd for $C_{30}H_{28}O_2S_3$: C, 69.73; H, 5.46; O, 6.19; S, 18.62. Found: C, 69.61; H, 5.52; S, 18.53.

2,5″-Bis(4-butoxyphenyl)-2,2′:5′,2″-terthiophene (dbo-P3TP). The same procedure as that for dip-P3TP was used. Instead of flashing through a column, the compound was further purified by vacuum sublimation to give an orange solid (yield = 74%). Anal. Calcd for $C_{32}H_{32}O_2S_3$: C, 70.55; H, 5.22; O, 5.87; S, 17.66. Found: C, 70.43; H, 5.22; S, 17.59.

2,5″-Bis(4-hexyloxyphenyl)-2,2′:5′,2″-terthiophene (dho-P3TP). The same procedure as that for dip-P3TP was used. The bright orange precipitate (yield = 76%) was filtered off, washed with methanol and chloroform, and further purified by vacuum sublimation. Anal. Calcd for $C_{36}H_{40}O_2S_3$: C, 71.96; H, 6.71; S, 16.01; O, 5.32. Found: C, 71.84; H, 6.68; S, 15.83.

2,5″-Bis(4-oxtyloxyphenyl)-2,2′:5′,2″-terthiophene (doo-P3TP). The same procedure as that for dip-P3TP was used to yield a bright orange precipitate (yield = 79.1%). Anal. Calcd for $C_{40}H_{48}O_2S_3$: C, 73.12; H, 7.36; O, 4.87; S, 14.64. Found: C, 72.83; H, 7.14; S, 14.37.

2,5″-Bis(4-butylphenyl)-2,2′:5′,2″-terthiophene (db-P3TP). To a solution of 2-(4-butylphenyl)-4,4,5,5,-tetramethyl-[1,3,2]dioxaborolane (1.10 g, 4.22 mmol) and 2,5″-dibromo-2,2′:5′,2″-terthiophene (0.85 g, 2.11 mmol) dissolved in toluene (15 mL) was added potassium carbonate (2.91 g, 21.1 mmol) dissolved in water (50 mL) followed by the addition of phase-transfer agent Aliquot 336 (0.85 g, 2.11 mmol). The mixture was bubbled with nitrogen for 15 min. Then, tetrakis(triphenylphosphine)palladium(0) (120 mg, 0.10 mmol) was added, and the mixture was bubbled with N_2 for an additional 10 min. The mixture was heated to 85 °C for 20 h under nitrogen. The bright yellow precipitate (yield = 66%) was filtered off, washed with methanol and chloroform, and further purified by vacuum sublimation. Anal. Calcd for $C_{32}H_{32}S_3$: C, 74.95; H, 6.29; S, 18.76. Found: C, 74.93; H, 6.02; S, 18.69.

2,5″-Bis(4-octylphenyl)-2,2′:5′,2″-terthiophene (do-P3TP). The same procedure as that for db-P3TP was used. The bright yellow precipitate was filtered off, washed with methanol and chloroform, and further purified by vacuum sublimation (yield = 80%). Anal. Calcd for $C_{40}H_{48}S_3$: C, 76.87; H, 7.74; S, 15.39. Found: C, 76.82; H, 7.65; S, 15.46.

2,5″-Bis(4-*tert*-butoxyphenyl)-2,2′:5′,2″-terthiophene (dtbo-P3TP). The same procedure as that for db-P3TP was used. The deep-orange compound was purified by Soxhlet extraction in chloroform to give a gold-colored solid (yield = 57%). Anal. Calcd for $C_{32}H_{32}O_2S_3$: C, 70.55; H, 5.92; O, 5.87; S, 17.66. Found: C, 70.76; H, 5.94; S, 17.61.

2-(4-Butylphenyl)-4,4,5,5,-tetramethyl-[1,3,2]dioxaborolane. To a two-neck 100 mL round-bottom flask was added 4-bromo-1-*n*-butylbenzene (1.00 g, 4.7 mmol), bis(pinacolato)diboron (1.30 g, 5.11 mmol), and potassium acetate (1.38 g, 14.1 mmol). A volume of 50 mL of anhydrous DMSO was added via syringe, then the solution was bubbled with N_2 for 20 min. 1,1′-Bis(diphenylphosphino)ferrocene−$PdCl_2$ (0.23 g, 0.28 mmol) was then added, and the solution was heated to 80 °C for 24 h. The solution was extracted with 50 mL aliquots of CH_2Cl_2 five times, dried over $MgSO_4$, and evaporated to yield a clear liquid (1.10 g, yield = 90%). ^{1}H NMR (200 MHz, $CDCl_3$): δ_H 7.67 (d, 2H, J = 8.0 Hz), 7.14 (d, 2H, J = 8.0 Hz), 2.56 (t, 2H, J = 7.14 Hz), 1.53 (m, 2H), 1.26 (m, 14H), 0.86 (t, 3H, J = 7.25 Hz).

2-(4-Octylphenyl)-4,4,5,5,-tetramethyl-[1,3,2]dioxaborolane. The same procedure as above was used to give a clear liquid (2.0 g, yield = 85%). ^{1}H NMR (200 MHz, $CDCl_3$): δ_H 7.67 (d, 2H, J = 7.9 Hz), 7.13 (d, 2H, J = 7.9 Hz), 2.55 (t, 2H, J = 7.7 Hz), 1.24 (m, 24H), 0.81 (t, 3H, 6.4 Hz).

2-(4-*tert*-Butoxyphenyl)-4,4,5,5,-tetramethyl-[1,3,2]dioxaborolane. The same procedure as above was used to give a clear liquid (1.8 g, yield = 92%). ^{1}H NMR (200 MHz, $CDCl_3$): δ_H 7.73 (d, 2H, J = 8.5 Hz), 6.99 (d, 2H, J = 8.5 Hz), 1.36 (s, 9H), 1.33 (s, 12H). ^{13}C NMR (500 MHz, $CDCl_3$, δ): 25.13, 25.28, 29.17, 79.06, 83.89, 123.32, 136.01, 158.65.

Results and Discussion

Synthetic Methodology. All oligomers were synthesized using Suzuki or Stille coupling reactions. The synthetic schemes for all derivatives are outlined in Schemes 1 and 2. When phenylboronic acid derivatives were not commercially available for the Suzuki reactions, phenylboronic ester intermediates were synthesized using Miyaura reaction conditions with a Pd(II) catalyst.[26] All reactions proceeded with high efficiency, with yields between 57% and 81% after vacuum sublimation (or column chromatography where solubility allowed). It is worth noting that both purification methods gave comparable purity by elemental analysis. P2TP molecules were all bright yellow in color, except for dip-P2TP, which was orange. All P3TP molecules were bright orange. Surprisingly, in general, it was found that the alkyl-P2TP molecules were slightly more soluble than the alkoxy-P2TP molecules. None of the P3TP molecules, except dtb-P3TP, were soluble enough for NMR measurements at room temperature in $CDCl_3$. All of the P2TP and P3TP derivatives (except dmo-P2TP) had a solubility greater than 5 mg/mL in chlorobenzene at elevated temperature, which is among the most soluble for any linear oligothiophene or co-oligothiophene system.

Cyclic Voltammetry. To study the electronic influence of both core and side-chain substitution, the oxidation potential of each derivative was measured using cyclic voltammetry. From this data, the HOMO energy levels of each derivative were estimated similar to previous literature-reported methods.[27] Each value is referenced to the ferrocene/ferrocenium redox couple (HOMO level = −4.8 eV) which was used as an internal standard. Two reversible oxidations were observed for all molecules except alkyl-P2TP compounds, which only showed one reversible oxidation. Figure 1 shows a plot of the first oxidation potential for the molecules according to their structural motif (P2TP vs P3TP, alkyl vs alkoxy). All molecules within each category had very similar oxidation potentials with small variance. Alkyl-P2TP molecules showed the highest oxidation potential at 0.56 V (lowest energy HOMO level estimated at −5.36 eV). The addition of a thiophene ring to the conjugated core lowers the oxidation potential by 0.11 V. The addition of an oxygen atom in the side chain also lowers the oxidation potential by 0.15 and 0.09 V for P2TP and P3TP molecules,

(26) Ishiyama, T.; Murata, M.; Miyaura, N. *J. Org. Chem.* **1995**, *60*, 7508−7510.
(27) deLeeuw, D. M.; Simenon, M. M. J.; Brown, A. R.; Einerhand, R. E. F. *Synth. Met.* **1997**, *87*, 53−59.

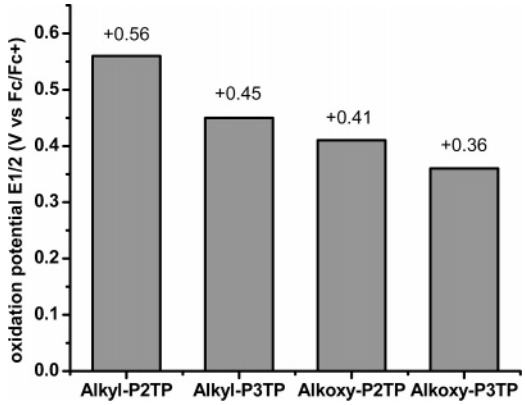

Figure 1. First oxidation potential of each category of molecules in the series.

respectively. For reference, pentacene measured by the same electrochemical setup had an oxidation potential of 0.1 V (HOMO level of −4.9 eV) versus the Fc/Fc^+ redox couple.

The fact that HOMO levels within a particular category (i.e., alkyl-P2TP or alkoxy-P3TP) are not only consistent with the hypothesis that variations in hydrocarbon side chains would not affect electronic levels in the conjugated core, but it also suggests that any differences or trends in mobility can be attributed to molecular packing as will be shown in the following sections.

AFM Nucleation Density/Grain Formation. Previous studies into the time-dependent growth mechanism of vacuum-deposited quarterthiophene and alkyl-substituted quarterthiophene films, performed by Ackermann et al.[28] and Campione et al.,[29] have shown that an incorporation of alkyl substituents on the semiconductor backbone shifts the growth mechanism from three-dimensional (3D) island to layer-by-layer growth (the different thin film growth mechanisms have been highlighted in recent literature).[30,31] The reason for this is twofold. First, the substitution lowers the substrate−molecule interaction. Second, the side chains give rise to increased lateral intralayer interactions and decrease the interlayer interactions between adjacent layers. This leads to larger, more interconnected grains, which enhances charge transport within the first few molecular layers of the organic semiconductor at the dielectric interface. A more detailed explanation of the role of side-chain substitution on thin film microstructure has been covered in a recent review.[32]

Films with 2 nm thickness were prepared on OTS-treated SiO_2 at a substrate temperature of 50 °C to investigate the influence of side-chain bulkiness on film morphology directly at the semiconductor/insulator interface, where the charge transport takes place. The corresponding AFM images are shown in Figure 2. With the linear side chains, the alkyl and alkoxy molecules exhibited two-dimensional (2D) growth on the surface, with a lower nucleation density evident in the alkyl-substituted molecules (Figure 2, parts a and b). The lower nucleation density (fewer grain boundaries) helps account for the increase in mobility for linear alkyl versus alkoxy side chains. The alkyl derivatives with branched side chains (dtb- and dip-P2TP) exhibited what looks like 3D (bulk) growth. This morphology probably explains the lower mobility observed with these derivatives. Figure 2, parts d and f, shows what appears to be a coexistence of two different phases in the branched alkoxy derivatives (dtbo- and dipo-P2TP). The step height of each island is 2.4 and 4.2 nm in Figure 2d. More investigation needs to be done in order to fully understand the reason for the two phases.

A similar morphological trend is observed with the series of P3TP derivatives. Figure 3, parts a and b, shows dtb-P3TP and dtbo-P3TP. As with the P2TP molecules, a similar difference in nucleation density is evident between alkyl- and alkoxy-substituted P3TP derivatives (Figure 3, parts c and d), but there was not a correlation between nucleation density and increasing linear side-chain length. The lower nucleation density we observed is consistent with the higher mobility within molecules that exhibit 2D growth (derivatives with linear side chains).

X-ray Diffraction. Table 1 lists the intermolecular *d*-spacing calculated from out-of-plane X-ray diffraction, which was performed using 45 nm thin films of each compound. The films were prepared on the same substrates with identical conditions as the transistor devices discussed below. Also listed are the MM2-minimized lengths calculated of each molecule, which were estimated using CS ChemBats3D Pro 7.0. The longer side-chain oligomers appear to have *d*-spacing lengths approximately equal to that of their molecular length. This is in contrast to the shorter/bulkier side-chain oligomers (dmo-P2TP, dtb-P2TP), which have *d*-spacing lengths that are 50% and 75% of their molecular length, implying either a significant tilt angle with respect to the substrate surface or side-chain interdigitation of adjacent molecular layers.

Device Parameters. Tables 2 and 3 show the device parameters for OFET devices fabricated from the phenylene−thiophene oligomers. All compounds show typical p-channel transistor properties, with representative current−voltage characteristics shown in Figure 5, parts a and b, for db-P2TP and db-P3TP, respectively. A few general observations are worth noting. First, field-effect mobility was observed for every derivative except dmo-P2TP. Second, there was no apparent correlation between mobility and conjugated core length (P2TP vs P3TP). Most oligomers generally showed higher mobility at elevated substrate temperatures, the optimum temperature of which is shown in Tables 2 and 3, although P2TP derivatives could not be deposited at temperatures greater than 55−60 °C (the observed film was cloudy with no working device). Also, when dip- and dbo-P3TP were deposited at higher substrate temperatures (90 vs 50 °C), lower mobility was observed. In addition, for dho- and doo-P3TP, no differences were observed for higher deposition substrate temperature (90 vs 50 °C).

(28) Ackermann, J.; Videlot, C.; Raynal, P.; El Kassmi, A.; Dumas, P. *Appl. Surf. Sci.* **2003**, *212*, 26−32.
(29) Campione, M.; Borghesi, A.; Moret, M.; Sassella, A. *J. Mater. Chem.* **2003**, *13*, 1669−1675.
(30) Ruiz, R.; Choudhary, D.; Nickel, B.; Toccoli, T.; Chang, K. C.; Mayer, A. C.; Clancy, P.; Blakely, J. M.; Headrick, R. L.; Iannotta, S.; Malliaras, G. G. *Chem. Mater.* **2004**, *16*, 4497−4508.
(31) Verlaak, S.; Steudel, S.; Heremans, P.; Janssen, D.; Deleuze, M. S. *Phys. Rev. B* **2003**, *68*, 195409.
(32) Locklin, J.; Roberts, M. E.; Mannsfeld, S. C. B.; Bao, Z. N. *Polym. Rev.* **2006**, *46*, 79−101.

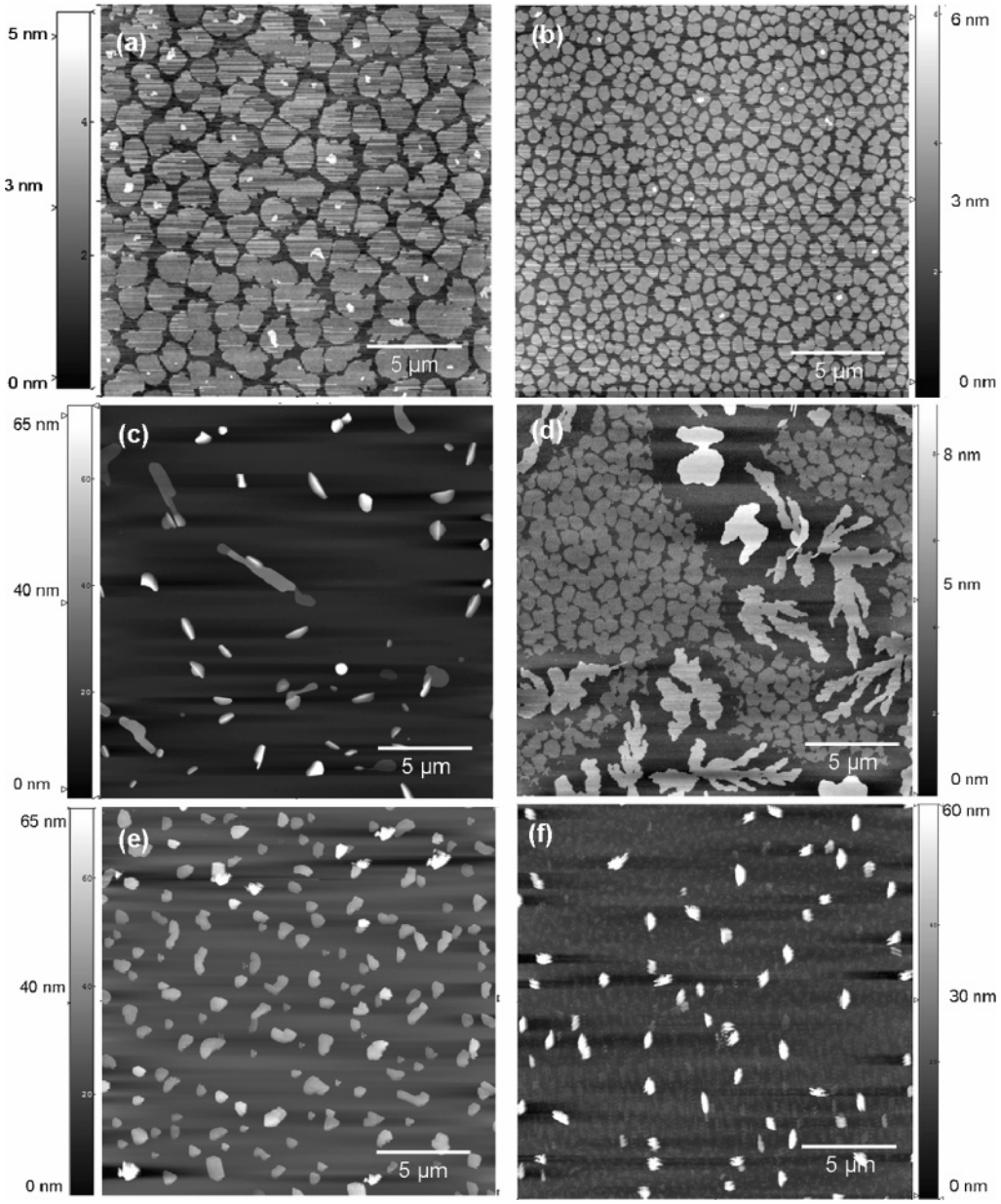

Figure 2. AFM topograph images of a 2 nm film on OTS-treated SiO_2 (deposited at $T_D = 50$ °C) of (a) db-P2TP, (b) dbo-P2TP, (c) dip-P2TP, (d) dipo-P2TP, (e) dtb-P2TP, and (f) dtbo-P2TP. Each image is 20 μm × 20 μm.

One of the goals of this study was to investigate the influence of introducing the alkoxy functionality into the side chain on the electrical properties of the molecule. Figure 4a−c presents the data for both types of side-chain functionality on the P2TP conjugated core. Figure 4c shows that for P2TP derivatives, alkyl-substituted molecules have more negative threshold voltages than their alkoxy-substituted counterparts with the same alkyl chain length. This is consistent with the observation that alkoxy-substituted molecules have higher energy HOMO levels, which makes them easier to oxidize or lowers the required gate voltage to turn on the device. In general, P3TP derivatives have lower threshold voltages than their P2TP counterparts, but the trend is not as clear due to the large spread of threshold voltage values calculated for each category. The fact that threshold voltage also varies greatly between trial runs is due to several factors including but not limited to atmospheric doping, morphological defects, dielectric surface functionality, and contact resistance.[33] Doping and trapping in organic semiconductors can result from a variety of reasons including oxidized molecules and the presence of impurities.[34] In addition, it appears that, as the bulkiness of the side chain decreases (*tert*-butyl > isopropyl > *n*-butyl), the mobility increases for both the alkyl- and alkoxy-P2TP derivatives, as well as a further increase in mobility as the length of the linear side chain increases from C4 to C8.

Figure 4d−f shows the electronic parameters for the alkyl- and alkoxy-P3TP derivatives. Interestingly, Figure 4d shows the same increase in mobility as the side-chain aspect ratio increases, but the mobility values for alkyl-P3TP molecules

(33) Horowitz, G. *J. Mater. Res.* **2004**, *19*, 1946−1962.
(34) Chua, L. L.; Zaumseil, J.; Chang, J. F.; Ou, E. C. W.; Ho, P. K. H.; Sirringhaus, H.; Friend, R. H. *Nature* **2005**, *434*, 194−199.

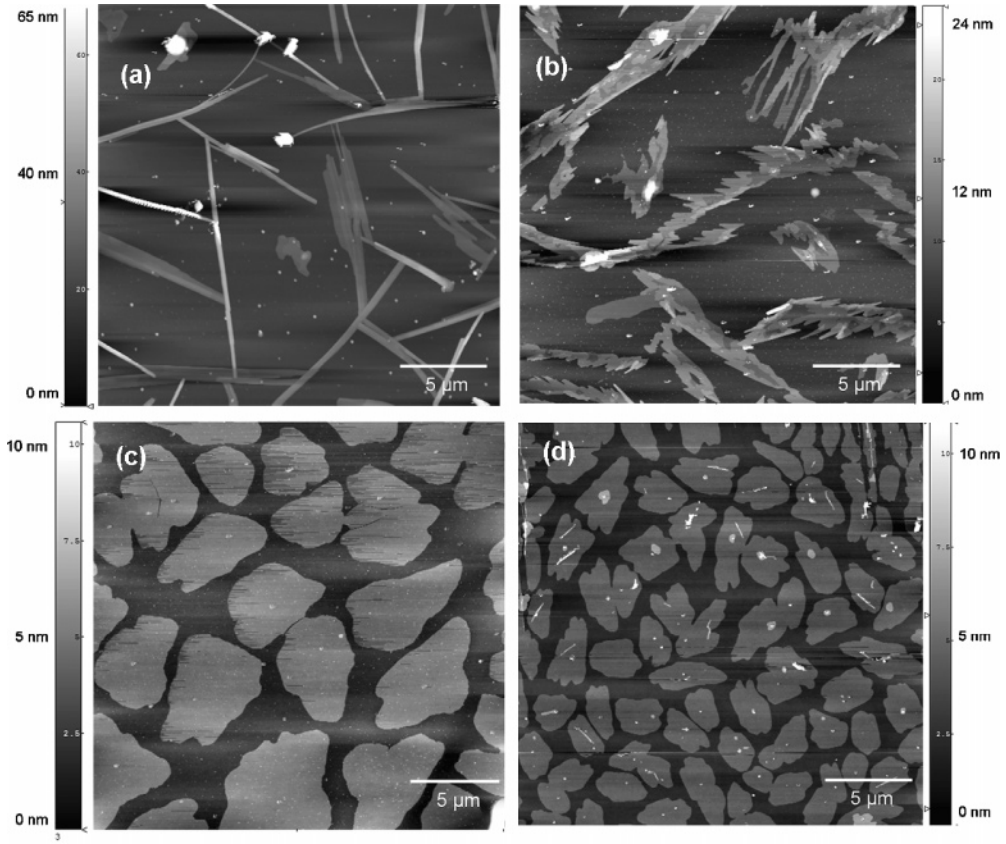

Figure 3. AFM topograph images of a 2 nm film on OTS-treated SiO_2 (deposited at $T_D = 50$ °C) of (a) dtb-P3TP, (b) dtbo-P3TP, (c) db-P3TP, and (d) dbo-P3TP. Each image is 20 μm × 20 μm.

Table 3. Mobility, On/Off, and Threshold Voltage Data for P3TP Molecules

molecule	mobility ($cm^2\ V^{-1}\ s^{-1}$)	on/off	V_T (V)	substrate temp (°C)
dip-P3TP	0.055 ± 0.0004	2×10^5	-11.9 ± 0.4	50[a]
dtb-P3TP	0.015 ± 0.0015	4×10^4	-0.05 ± 1.3	100
db-P3TP	0.14 ± 0.0008	3×10^6	-5.6 ± 1.5	125
do-P3TP	0.019 ± 0.001	2×10^5	-8.5 ± 1.6	90
dpo-P3TP	0.016 ± 0.0002	6×10^4	-16 ± 0.25	90
dipo-P3TP	0.001 ± 0.00003	1×10^3	-18.5 ± 0.4	40
dtbo-P3TP	0.008 ± 0.0005	2×10^5	-5.8 ± 1.7	90
dbo-P3TP	0.12 ± 0.002	2×10^4	-2.3 ± 1.2	50[b]
dho-P3TP	0.06 ± 0.0007	1×10^4	-2.4 ± 1.4	60[c]
doo-P3TP	0.09 ± 0.001	2×10^4	-7.3 ± 0.6	50[c]

[a] Thin films of dip-P3TP deposited at 90 °C gave lower mobility by a factor of 10 ($\sim 3 \times 10^{-3}$ $cm^2\ V^{-1}\ s^{-1}$). [b] Thin films of dbo-P3TP deposited at 90 °C gave lower mobility (~ 0.08 $cm^2\ V^{-1}\ s^{-1}$). [c] Thin films of dho- and doo-P3TP deposited at 90 °C gave no significant difference in mobility, on/off, or threshold values.

peak at shorter chain lengths than alkyl-P2TP compounds. Since the P2TP molecules are shorter, this may suggest that there is an optimal molecular length at which maximum mobility is achieved.

Figure 5 shows the calculated field-effect mobility as a function of *n*-alkoxy-P2TP/P3TP side-chain length. Threshold voltage as a function of side-chain length did not follow a consistent trend. On/off ratios display a very interesting trend with alkoxy-P2TP molecules consistently exhibiting higher ratios than alkoxy-P3TP in addition to higher ratios with increasing side-chain length for P2TP. Generally, higher mobility is observed with longer side chains in P2TP compounds and P3TP molecules show a peak in mobility with intermediate side-chain lengths ($(CH_2)_{4-6}$).

Figure 4a exhibits the clearest trend relating side-chain bulkiness and mobility. It appears that the less bulky side chain P2TP molecules have higher mobilities regardless of the presence of a bridging oxygen. It is very likely that the bulky side chains prevent close packing of the molecules in the thin film and thus reduce the $\pi-\pi$ overlap needed for intermolecular charge transport. Perhaps more important than the effect of orbital overlap on mobility is the presence and morphology of grain boundaries. At a macroscopic scale, continuity of grain boundaries determines the ease with which electrons or holes can hop between crystal grains. When vacuum depositing organic semiconductors, it is highly unlikely that a single crystal will be grown across the 200 μm channel. Thus, in order for holes (in the case of p-type semiconductors) to move from one electrode to the other, it is necessary for them to cross multiple grain boundaries. Due to the discontinuity in conjugation across these boundaries, it is the resistance inherent in this transport mechanism that most likely affects hole mobility in the thin film. In support of this, the AFM images in Figures 2 and 3 consistently show higher nucleation densities as the side chain increases in bulkiness (*n*-butyl < isopropyl < *tert*-butyl). Higher nucleation densities mean more grains per unit area and, thus, more energetic boundaries to cross per unit length. The high-mobility compounds (db-P2TP, $\mu = 0.14$ $cm^2\ V^{-1}\ s^{-1}$; dbo-P2TP, $\mu = 0.07$ $cm^2\ V^{-1}\ s^{-1}$) grew monolayer grains, suggestive of a 2D growth mechanism. dipo-P2TP ($\mu = 0.046$ $cm^2\ V^{-1}\ s^{-1}$) also displays a similar growth mechanism; however, the appearance of polymorphic thin film states introduces irregular grain boundaries and may

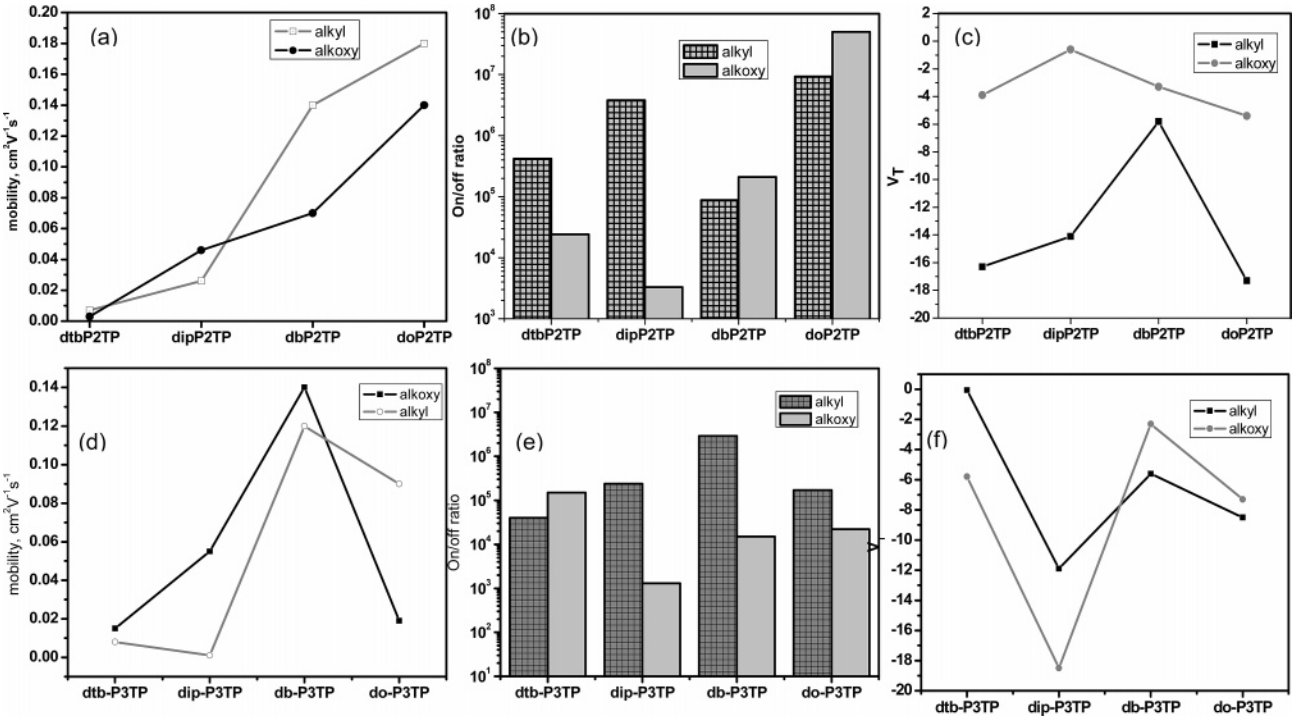

Figure 4. Averaged electronic parameters plotted as a function of side-chain functionality for the P2TP (a−c) and P3TP (d−f) series of compounds. Mobility (a and d): as the bulkiness of the side chain decreases, the mobility increases. On/off ratio (b and e): no consistent trend between alkyl and alkoxy derivatives. Threshold voltage (c and f): more negative threshold voltages for alkyl- vs alkoxy-P2TP derivatives. There is no consistent numerical trend observed with the P3TP derivatives.

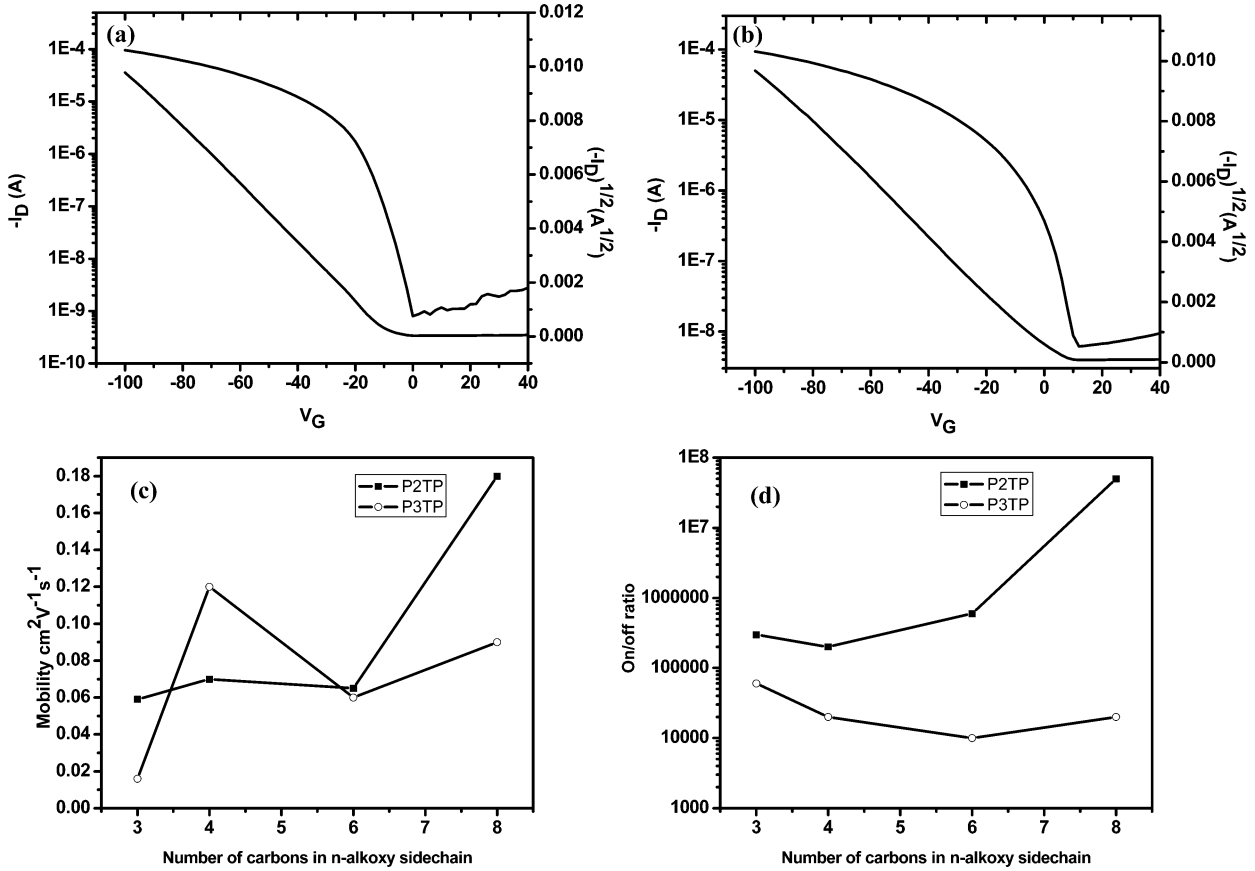

Figure 5. (a). Transfer curve for db-P2TP at $T_D = 40$ °C. (b). Transfer curve for db-P3TP at $T_D = 50$ °C. Mobility (c) and on/off ratio (d) as a function of *n*-alkoxy side-chain length.

explain the lower mobility compared to that of db-P2TP and dbo-P2TP. The lowest mobility compound in the group, dtbo-P2TP ($\mu = 0.003$ cm^2 V^{-1} s^{-1}), displayed very high nucleation density with very sharp and irregular grain boundaries. It should be noted that the highest mobility does not always correlate with the largest grain size. This has been

observed with pentacene on SiO_2 with different surface treatments by several groups.[35,36] Recently, Yang et al. used conducting AFM to demonstrate that the growth of the first pentacene monolayer strongly influences the structure of grain boundaries within the first layer.[37] The orientation of molecules at grain boundaries, or the crystallinity within grains, also plays an important role in charge transport.

The X-ray data also revealed the difference between the thin film molecular packing of short side-chain molecules compared with that of the longer side-chain ones. It is expected that both dmo-P2TP and dtbo-P2TP have a significant tilt angle to the substrate surface due to the significant difference in *d*-spacing and molecular length. Although it is inaccurate to calculate a tilt angle due to the possible existence of interdigitation or polymorphism, it is reasonable to conclude that these bulky side-chain molecules have a larger tilt angle than that of the long straight side-chain compounds. This increase in tilt angle may explain the generally lower mobility observed in these molecules (dmo-P2TP, no observed mobility; dtb-P2TP, $\mu = 0.007$ cm^2 V^{-1} s^{-1}).

Conclusions

This study has demonstrated the facile synthesis of many high-performance phenylene−thiophene oligomers. Five compounds have mobilities higher than 0.1 cm^2 V^{-1} s^{-1}, and several of them had on/off ratios of 10^6 or higher. do-P2TP shows the most potential with a field-effect mobility of 0.18 cm^2 V^{-1} s^{-1} and on/off ratio of 10^7 with a substrate deposition temperature of 50 °C. At these low deposition temperatures, the molecule could be compatible with all currently used plastic substrates for flexible active matrix displays. In addition to high performance characteristics, some of the compounds are soluble enough to be flashed through a silica column. Despite the attempt to include a large number of variations in side-group structure to these series of molecules, many more combinations and comparisons can be made. Future work includes fabrication of bottom contact transistors by solution casting. Field-effect mobilities as high as 0.08 cm^2 V^{-1} s^{-1} have been observed from solution casting techniques with these derivatives, and this data will be reported elsewhere. This study has highlighted only a few of the unlimited number of structural variations that can be synthesized, and the results of the correlation between morphology and device performance will aid in designing novel organic semiconductors that are tailored for specific application.

Acknowledgment. A.S. acknowledges the Stanford School of Engineering for a summer research grant. J.L. would like to thank the Intelligence Community Postdoctoral Fellowship for financial support. Z.B. acknowledges partial financial support from the Finmeccanica Faculty Scholar Award, the 3M Faculty Award, the Center for Polymeric Interfaces and Macromolecular Assemblies (NSF-Center MRSEC under Award No. DMR-0213618).

CM070117N

(35) Knipp, D.; Street, R. A.; Volkel, A.; Ho, J. *J. Appl. Phys.* **2003**, *93*, 347−355.
(36) Yanagisawa, H.; Tamaki, T.; Nakamura, M.; Kudo, K. *Thin Solid Films* **2004**, *464−65*, 398−402.
(37) Yang, H. C.; Shin, T. J.; Ling, M. M.; Cho, K.; Ryu, C. Y.; Bao, Z. N. *J. Am. Chem. Soc.* **2005**, *127*, 11542−11543.